A Fast Mesh-Growing Algorithm for Manifold Surface Reconstruction

Luca Di Angelo[1], Paolo Di Stefano[2] and Luigi Giaccari[3]

[1]University of LõAquila, luca.diangelo@univaq.it
[2]University of LõAquila, paolo.distefano@univaq.it
[3]ANSYS Germany Gmbh, luigi.giaccari@ansys.com

ABSTRACT

In a previous paper these authors presented a new mesh-growing approach based on the *Gabriel 2 – Simplex* (*G2S*) criterion. If compared with the *Cocone* family and the *Ball Pivoting* methods, *G2S* demonstrated to be competitive in terms of tessellation rate, quality of the generated triangles and defectiveness produced when the surface to be reconstructed was locally flat. Nonetheless, its major limitation was that, in the presence of a mesh which was locally non ð flat or which was not sufficiently sampled, the method was less robust and holes and non ð manifold vertices were generated. In order to overcome these limitations, in this paper, the performance of the *G2S* mesh-growing method is fully improved in terms of robustness. The performances of the new version of the *G2S* approach (in the following *Robust G2S*) has been compared with that of the old one, and that of the *Cocone* family and the *Ball Pivoting* methods in the tessellation of some benchmark point clouds and artificially noised test cases. The results obtained show that the use of the *Robust G2S* is advantageous, as opposed to the other methods here considered, even in the case of noised point clouds. Unlike the other methods, the one which is proposed preserves manifoldness and geometric details of the point cloud to be meshed.

Keywords: surface reconstruction, triangular meshes, reverse engineering.
DOI: 10.3722/cadaps.2013.197-220

1 INTRODUCTION

The approximation of a 3D surface from its point samples is a very important issue in the scientific and engineering realms. Depending on the application, various formulations to this problem can be furnished with various requirements in the input and the output. Among those formulations, the applications of triangular meshes obtained from scanned point clouds are wideðranging and include Reverse Engineering, Collaborative Design, Inspection, Computer Vision, Dissemination of Museum artifacts, Medicine, Movie Special Effects, Games and Virtual Worlds. For all the applications, the meshes obtained must match the original data set in terms of geometric and topological criteria. Those objectives are hard to be achieved since scanned point clouds are typically noisy and badly sampled in some areas difficult to access and they have a non-uniform density. Nowadays, these critical aspects are only partially limited thanks to the introduction of scanning systems which offer high resolutions with a measuring accuracy as high as 10 εm. As a direct result, the necessity to manage very large data sets is becoming even more important. The typical triangulation speed of the methods presented in literature may not be enough for the tessellation of a cloud with over one million points. Furthermore, as regards the defectiveness produced, even the methods which are considered to be very robust can generate non**ð**manifold vertices. It is important to highlight the fact that much of the software used for mesh elaboration may not work in the presence of this type of vertices.

These authors have recently proposed a new mesh-growing method based on the Gabriel 2 **ð** Simplex (*G2S*) criterion. The results obtained are very promising since they demonstrate that this method makes it possible to tessellate quickly clouds with over one million points even by using a laptop. Its major limitation is however that, in the presence of a mesh which is locally non**ð**flat or which is not sufficiently sampled, the method is less robust and therefore holes and non**ð**manifold vertices are generated. We should bear in mind the fact that the mesh may be unusable without the deletion of this kind of vertices, which has to be carried out without compromising the areas which have been correctly reconstructed.

In order to overcome these limitations, and as it is going to be shown in this paper, the performance of the G2S mesh-growing method is fully improved in terms of robustness. To this end, an original priority queue for the driving of the front growth and a post-processing to efficiently erase the non**ð**manifold vertices are proposed. The improved method has been tested for the tessellation of some benchmark point clouds and artificially noised test cases. The results derived from these experiments are critically discussed hereinafter.

2 RELATED WORKS

Various algorithms to tessellate point clouds have been proposed throughout literature. Some recent exhaustive overviews are available in [1] and [2]. Surface reconstruction algorithms are generally divided into three categories:

- *implicit*;
- *Voronoi/Delaunay-based*;
- *mesh growing - based*.

2.1 Implicit Methods

In implicit methods the surface reconstruction is obtained by extracting the nominally zero **ð** level set of a properly defined implicit function $f(\mathbf{p})=0$ (where $\mathbf{p}$ is either the whole point cloud or only a part of it), formulated so as to be negative inside the point cloud object and positive outside. Typically, the tessellated surface is obtained by applying the *Marching cubes algorithm* [3] to the iso-surfaces. The most important methods belonging to this group differ in whether the implicit function is defined:

- as the sum of radial basis functions (RBF) centred at the points [4], [5];
- as a set of constraints that force the function and its gradient to assume given values at the sample points (Moving Least Squares) [6], [7], [8];
- as a Poisson problem [9].

A typical shortcoming of implicit methods is that they are sensitive to the outliers. With a view to overcoming this limitation, some new methods ([10], [11], [12] and [13]), based on stratified reconstruction strategies, have been recently developed.

By and large, all these methods, on the one hand, carry out a watertight surface reconstruction even in the case of sparse and noisy data but, on the other hand, require many computations and, sometimes, even the surface normal at each data point. Since the final surface may not pass through all the points, the computational time increases as the fitting accuracy increases. Finally, as pointed out by Yang et al. in [8], the resulting mesh must be further refined and optimised.

2.2 Voronoi/Delaunay-based Methods

This group includes algorithms that compute a volume tetrahedralisation by means of a 3D Delaunay triangulation of the sample points. The most important methods presented in the related literature ([14], [15], [16], [17], [18], [19], [20] and [21]) differ essentially in the way they remove the tetrahedra and build the external triangular mesh. In the *Crust* method, proposed by Amenta et al. in [14], the set of *candidate triangles* (called *Crust*) are those having three vertices which are not poles (for each point **p** of the cloud the *poles* are the two Voronoi vertices which are farthest from **p**). Since the *Crust* is still not a manifold, in order to extract a topologically correct surface, a *walking strategy* is employed in *candidate triangles*. The worst time complexity of the *Crust* algorithm is Ū(m^2), where m is the number of points plus poles. In order to reduce running time and memory consumption, while still providing the same theoretical guarantees, Amenta et al. in [15] proposed an improvement of the *Crust* algorithm, which they called *Cocone*. The *candidate triangles* are those triangles inside the *Cocone region*, which is the complement of a double cone which has its apex at the point under analysis (**p**) and an assigned opening angle and whose axis is the normal at **p**. The *Cocone*'s worst time complexity is Ū(n^2), where n is the number of points. As pointed out by Chang et al. in [2], the theoretical guarantee of obtaining a correct reconstruction with the *Crust* and *Cocone* methods is only possible as long as the point cloud is well sampled. Dey and Goswami proposed other *Cocone* versions, one suited to provide a watertight closed surface reconstruction, which they called *Tight Cocone* [16] and the other suited for noisy data called *Robust Cocone* [17]. Dey et al. in [18] proposed the *Super Cocone* algorithm so as to manage large amounts of data. In that method, the entire set of sample points is partitioned into smaller clusters using an octree subdivision, and the *Cocone* algorithm is applied to each cluster separately. A further evolution of the *Crust* is the *Power Crust* proposed by Amenta et al. in [19]. This algorithm can generate a watertight mesh for any point cloud which is sampled enough but it could be non-manifold. Furthermore, sharp edges or noisy data can result in defectiveness.

Gopi et al. in [22] proposed a different approach which, for each sample point, provides the projection of the neighbouring points onto the approximating tangent plane as well as the tessellation of the projections by means of a 2-D Delaunay triangulation. The 2D edges obtained are then applied to 3D space. With a view to enhancing the performance of the Delaunay-based methods, Cohen-Steiner and Da in [20] proposed the *Greedy algorithm*, which selects the triangles sequentially. The selection of *candidate triangles* is carried out by the *plausibility grade*, which is an empirical function of the circumradius and the dihedral angle between adjacent triangles. As stated by Cazals and Giesen in [23], this method òmay fail to interpolate all points or to provide a closed surface essentially due to the presence of sliversó.

2.3 Mesh-growing Methods

In mesh ð growing approaches the surface reconstruction starts with a seed triangle and the meshed area is grown by pushing the fronts ahead using some criteria. Bernardini et al. [24] introduced the *Ball Pivoting Algorithm* (*BPA*), by which the front grows as a ball of user-defined radius pivots around the front edge. When the ball touches three points, a new triangle is formed. This method affords a correct triangulation for any uniform data point, also in presence of noise, but it has some difficulties in the tessellation of concave areas with little curvature radius. Huang and Menq in [25] proposed an algorithm which, for each front edge, projects the k-nearest points of two endpoints onto the plane that is defined by the triangle adjacent to the front edge. Any point generating triangles whose edges intersect edges of already-existing triangles is discarded. Of the points which are retained, the point showing the minimum sum of distances from the front-edge endpoints is chosen. Nonetheless, as pointed out by Lin et al. in [26], this algorithm presents some shortcomings. In order to overcome them, Lin et al. in [26] introduced the *Intrinsic Property Driven* (*IPD*) algorithm, which improves the way of searching for the points to be triangulated. As stated by Chang et al. in [2], all the methods based on mesh-growing approaches are fast, efficient and simple to implement but they, however, may fall short whenever two surfaces are either close together or near sharp features. More recently, Li et al. in [1] proposed a method based on a *Priority Driven* approach that evaluates shape changes from an estimation of the original surface that is made at the front of the mesh-growing area. The experimental results in [1] evidenced that the triangulation speed of the method was higher than that of the *Ball Pivoting* and the *Cocone*. However, no reckoning was made of the defectiveness generated by the method. Finally, in [27] these authors put forth a new mesh growing approach based on the *Gabriel 2 – Simplex* (*G2S*) criterion: *A triangle is a G2S if its smallest circumscribing ball is empty*. This criterion degenerates into the classical 2D Delaunay if all the points are coplanar. As a direct consequence, the flatter the surface appears to be locally, the better is the guarantee of a good reconstruction. More generally, the theoretical guarantee of a good reconstruction can be founded on the following theorem demonstrated by Dyer et al. in [29]: *A Gabriel mesh is a Delaunay mesh*. In other words, any mesh in which every triangle verifies the *G2S* criterion verifies also the 3D *Delaunay* one. As opposed to the 2D and 3D classical Delaunay criterion, for a given data set, the *G2S* triangulation is not unique and depends on the chosen seed triangle. The *G2S* criterion has already been used in some tessellation methods presented in literature. Ruiz et al. in [30] used it as a basis for a method for parametric surface meshing. This method cannot be used directly for the triangulation of point clouds since it is based on information such as the pre-image in a parametric space, the boundary, and local curvatures. Cohen-Steiner and Da in [20] and Ma et al. in [21] used the *G2S* criterion in order to select the external triangular facets of tetrahedra coming from a 3D Delaunay triangulation. The method proposed by Di Angelo et al. in [27] applied the *G2S* criterion directly to a point cloud so as to identify triangles pertaining to the external surface. This method has proven to be competitive in terms of tessellation rate, quality of the generated triangles and defectiveness produced when the surface to be reconstructed is locally flat. Nonetheless, in the presence of a noisy mesh or a mesh which is locally nonǒflat or which is not sufficiently sampled, the method generates defectiveness such as holes and nonǒmanifold vertices.

3 THE GABRIEL 2 – SIMPLEX CRITERION BASED METHOD

The mesh-growing method proposed in [27] consists of the following steps:

step 1. Import of the point cloud;
step 2. Building of a specific data structure to speed up the search for the nearest point;
step 3. Search for the seed triangle;
step 4. Surface triangulation.

The first step involves importing the point cloud which pertains to a continuous surface in the form of the coordinates x, y, z. Other information, such as the normal at points, is not required. All the points from the cloud are held in an original hash table data structure, applied to an improvement of the typical space division approach ([31] and [32]), which makes it possible a more efficient search for the nearest neighbourhoods. Then, the seed triangle is selected by using a new approach which guarantees that it pertains to smooth features of the external surface of the point cloud. Starting from the seed triangle, the meshed area grows, coherently with a manifold surface, by pushing the fronts ahead using the *G2S* criterion.

3.1 Selection of the Seed Triangle

The *G2S* criterion being applied does not ensure that the triangles belong to the external surface. In fact, the *G2S* triangles can either lie on the external surface or be transversal to it. Thus, as it happens with the other mesh-growing approaches, the selection of the seed triangle is an important aspect of the proposed method.

The seed triangle is selected based on an original strategy consisting of the following sub-steps:

Step 3.1. A point of the cloud is randomly chosen.

Step 3.2. Its nearest neighbour point is searched for, and an edge is formed between these two points.

Step 3.3. The third point of the triangle is searched for within a sphere centred at the midpoint of the edge and whose radius is k-times the length of the edge (k can be either a user-defined parameter or a default value).

Step 3.4. Each point in the range is connected to the edge in order to form a triangle.

Step 3.5. Selection of the seed triangle. The seed triangle verifies the *G2S* criterion and the points contained in the infinite cylinder passing through its three vertices, and having the axis parallel to its normal, are all above or all under the triangle (figure 1).

The procedure is repeated until a triangle, satisfying the conditions in step 3.5 is found. The cylinder test also excludes any *G2S* triangles which are in correspondence of sharp points.

3.2 G2S Criterion-based Triangulation

The edges of the seed triangle constitute the initial advancing front of the growing-mesh method. For each *free edge* ($\mathbf{e}_f$) (which are edges pertaining to only one triangle) of the growing front a triangle is generated according to the following procedure sub-steps:

Step 4.1: Identification of all the candidate points near $\mathbf{e}_f$.

Typically, the *reference point* is chosen among the *candidate points,* which are those inside a properly defined search region. In this paper the search region is a sphere having its centre (*search region centre*) lying on the plane of the *front triangle* on the axis of the *free edge* under analysis in the growing direction, and having the *search radius* as radius (figure 2). The *search radius* value affects tessellation quality and time. A low *search radius* keeps the search region near the front edge, so the method falls short in the meshing of under sampled areas. A high *search radius*, on the other hand, reduces the tessellation rate and sometimes generates defectiveness. An automatic approach has been implemented to set the *search radius* value. It changes the *search radius* value from an initial value (in the following test cases it is equal to the length of the *free edge* under analysis) to an assigned maximum value according to a given step value. The *search radius* is increased up to the maximum value if no points are found inside the search region. Since the *search region centre* lies on the same plane as the *front triangle*, the search method usually favours finding candidate points in the area wherein the surface is expected to grow. In typical practical situations, this prevents further controls that may cause the algorithm to slacken. Furthermore, this *search region* excludes from *candidate points* those points which are farther away or those points which could generate thin and slivery triangles. Finally, this criterion generally stops the front in the presence of sharp edges.

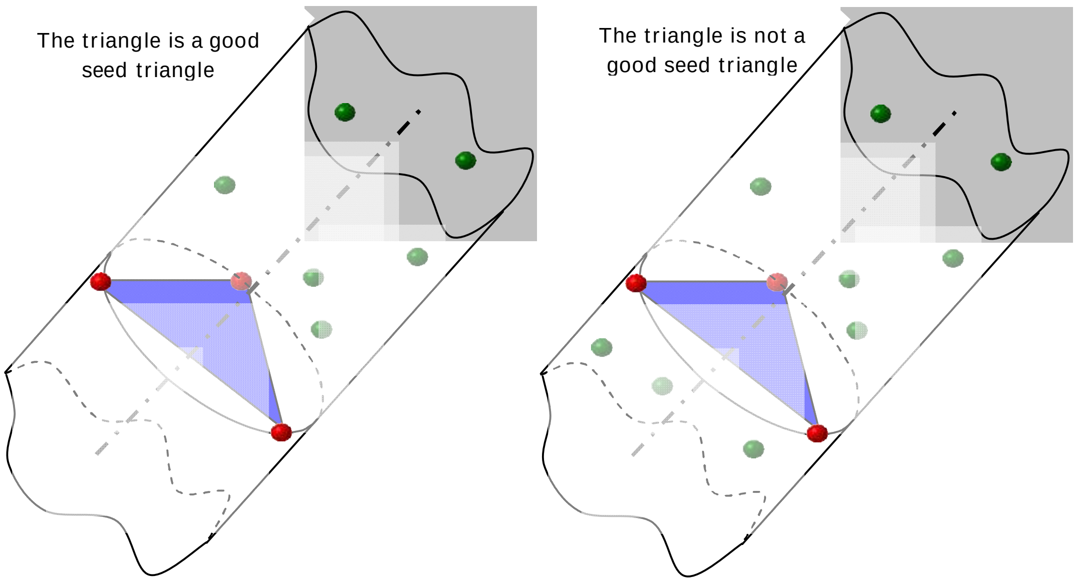
The triangle is a good seed triangle
The triangle is not a good seed triangle

Fig. 1: The cylinder test to select a seed triangle.

Step 4.2: Selection of the reference point in the search region.
When more than one point is found inside the search region ($\mathbf{cp}_1$, $\mathbf{cp}_2$ and $\mathbf{cp}_3$ in figure 3*a*), for each point the smallest sphere passing through it and the *front edge*'s points is traced. The point which verifies the *G2S* triangle is the *candidate point*. Then, the candidate triangle (figure 3*b*) is submitted to topological tests. In order to speed up the triangulation process, if only one point is found inside the *search region*, that point is directly assumed to identify a *candidate triangle* with the *free edge* ($\mathbf{e}_f$) without verifying whether or not it is a *G2S*. For a quasi-locally flat point cloud, the *candidate triangle* has a high probability of being *G2S*. Finally, if no point is found inside the search region, $\mathbf{e}_f$ is removed from the *free edges' queue* and it is classified as *boundary edge*.

Step 4.3: Topological tests and algorithm control.

Each of the new triangles retained is formed by the front edge ($\mathbf{e}_f$) and two further edges ($\mathbf{e}_1$ and $\mathbf{e}_2$). In order to check efficiently whether these two edges ($\mathbf{e}_1$ and $\mathbf{e}_2$) are really new or they already belong to other triangles, a data structure called *Point Edge Map* (*PEM*) is proposed which relates every point to its edges. For either edge ($\mathbf{e}_1$ and $\mathbf{e}_2$), the following conditions should be verified:

- If the edge already pertains to another triangle, the consistency of the orientation of the new triangle with the triangle sharing the edge must be verified.
- If this edge is new, it is added to the *Point Edge Map* and to the front queue and $\mathbf{e}_f$ is removed from the front queue.

The procedure ends when the *free edges' queue* is empty.

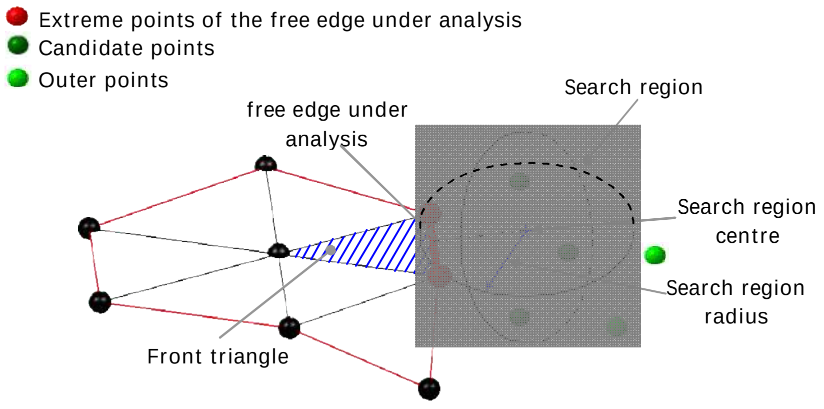

Fig. 2: The search regionís definition terms.

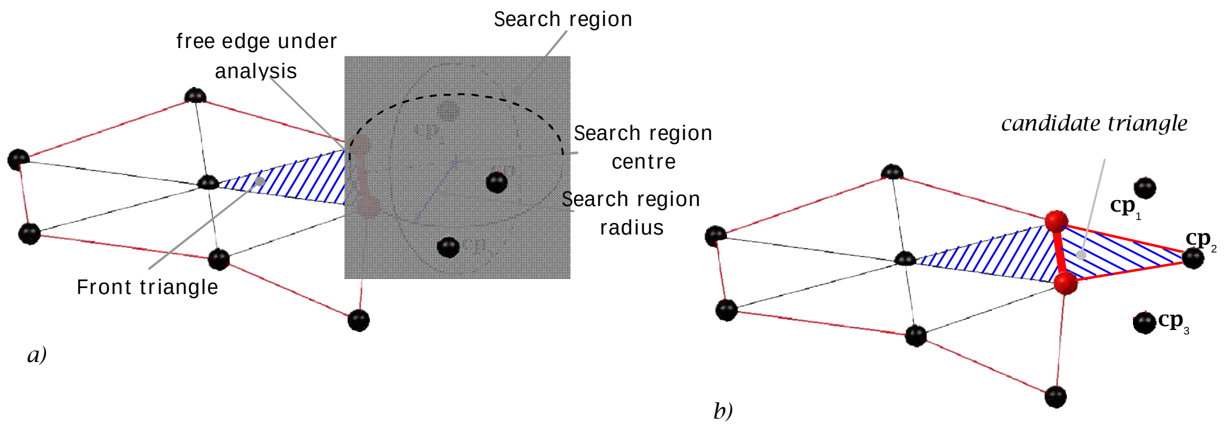

Fig. 3: Reference point selection.

3.3 Some Considerations

The theoretical basis of *G2S* is taken for granted by accepting the fact that point clouds can be considered locally flat, or, in other words, that the surface to be reconstructed is locally oriented, smooth, manifold, well sampled and not self-intersecting. Under this hypothesis, the *G2S* criterion works like a 2D Delaunay tessellation through which surface reconstruction is guaranteed. These requirements are not so restrictive anymore, especially since the advent of high-resolution nonð contact scanners which produce noise-free points clouds. More generally, as pointed out by Dyer et al. in [29], a *Gabriel mesh* (a mesh for which each triangle verifies the *G2S* criterion) is a *Delaunay mesh*. In [27] these authors already demonstrated it by analysing the typical benchmarks presented in the related literature:

- the triangulation speed of G2S is comparable with a traditional 2D Delaunay-based mesher and it is at least an order of magnitude higher than the other methods here considered;

- G2S produces triangles whose quality is similar to that of those triangles obtained by the Cocone methods and slightly better than the quality of the triangles obtained by the Ball Pivoting one;
- G2S can reproduce even the smallest details of well sampled surfaces, similarly to Cocone methods, also in concave areas of strongly nonðuniform point clouds where the Ball Pivoting method shows some problems;
- G2S does not produce nonðmanifold edges, self-intersecting triangles or slivers;
- as regards nonðmanifold vertices, holes and boundary edges, the quantity and the extension of defectiveness generated by the G2S tessellation are on average similar to those produced by the *Cocone* and the *Tight Cocone*;
- in the presence of a mesh which is locally nonðflat or which is not sufficiently sampled, G2S is less robust and holes and nonðmanifold vertices are generated.

4 CRITICAL ASPECTS IN THE G2S METHOD AND IMPROVEMENTS

As mentioned in the previous section, the *G2S* version proposed in [27] presents some critical aspects. In particular, in any area of a point cloud that is not locally flat or is not sufficiently sampled, *G2S* can generate:

- holes, which identify unmeshed area;
- a twisting of the surface;
- nonðmanifold vertices.

In order to eliminate non-manifold vertices, in literature some methods are proposed ([33] and [34]). Typically, these methods work as a step that is completely independent from the tessellation phase, by using static large data structures which could be inadequate to repair meshes with some millions of triangles.

This paper focuses on the improvement of the G2S performance as regards the generation of twisted *surfaces* and *non-manifold vertices*. The methods here proposed take advance from the data generated by the mesh growing algorithm and they can manage millions of triangles.

4.1 The Twisting of the Surface

In this paper, the *twisting of the surface* identifies the generation on the same body of different tessellated surfaces not having congruent normal (figure 4). This in turn generates holes with extended boundary edges since adjacent patches not having a congruent orientation cannot be merged. In order to solve this problem, an original *priority queue* is proposed. The main idea at the basis of the priority approach being presented is to mesh first those areas for which the front grows in the flattest way in the neighbourhood.

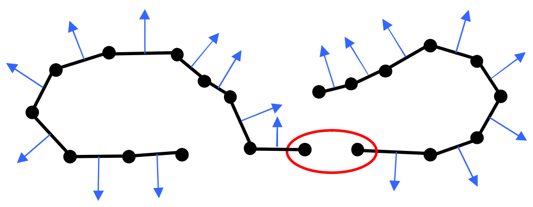
Fig. 4: The twisting of the surface.

In order to speed up the algorithm, a set of discrete values is adopted for a *priority index.* The strategy used involves the definition of:

- n priority levels for the search neighbourhood dimension, so that the smallest dimension has priority pl_d = 1 and the greatest has priority $pl_d = n$);
- m priority levels for flatness, measured as the angle (β) between the normal of the triangle containing the *free edge* under analysis (*front triangle*) and the *candidate* triangle (priority pl_f = 1 being assigned to β=0° and priority pl_f = m to β=180°).

The *priority index* (*PI*) is defined according to the following expression:

$$PI = m \cdot (pl_d - 1) + pl_f \tag{4.1}$$

Next, these edges are positioned in the queue by sorting, in ascending order, the value of *PV* calculated for the corresponding *candidate triangle*.

4.2 Non – manifold Vertices Elimination

In what follows, the triangles with at least one *boundary edge* are referred to as *boundary triangles* and the vertices, for which the incident triangles form more than one fan are referred to as *non-manifold vertices*. In this paper the two common types of *non-manifold vertices*, reported in the figure 5, are considered. In order to verify that a vertex is manifold, the sequence of triangles sharing the vertex is analysed. For this purpose, a specific data structure has been defined;

- a dynamic queue of edges (*deq*) containing the non-analysed edges which initially has n_e rows (n_e is the number of edges that are not boundary) and six columns: the edge label (e_i), its extreme points (p_f and p_l) and the triangles sharing the edge t_f and t_l);
- a n_v·4 matrix (*ptt*) (n_v is the number of vertices); in each row of *ppt* the sequence of adjacent triangles sharing the vertex (v_i) is represented by storing the first (*front*) and the last (*back*) triangle of the sequence and the number of the triangles found ($n_{t,a}$). A vertex is checked to be manifold if $n_{t,a}$ is equal to the number of triangles sharing the vertex.

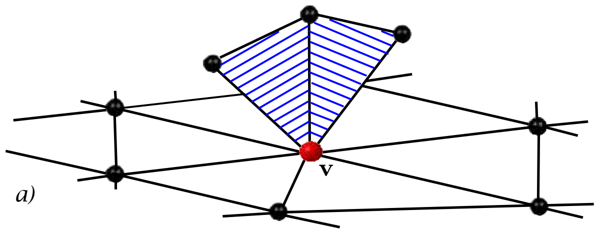

Fig. 5: Common types of non ð manifold vertices.

In order to explain this method, let us consider the mesh represented in figure 6a with the labels of the vertices, edges and triangles superimposed. First, the *deq* is filled with the edges of the mesh, except for the boundary ones (figure 6b) and in the *ptt* table, the labels of all vertices are added to the first column (figure 6c). The process starts by popping the first element off the queue ($\mathbf{e}_3$) and the corresponding labels of t_f ($\mathbf{t}_1$) and t_l ($\mathbf{t}_2$) are added to the related lines of the matrix (figure 6d). Then, the first element of the new queue (figure 6e) is popped off ($\mathbf{e}_6$). Since the trianglesõ labels associated with $\mathbf{v}_1$ for $\mathbf{e}_6$ ($\mathbf{t}_3$ and $\mathbf{t}_8$) are different from those reported in the corresponding row of the matrix, this edge is pushed to the end of the queue (figure 6f). If once the queue has been scanned through, no edges of intersection of one of two extreme triangles of the loop ($\mathbf{t}_1$ and $\mathbf{t}_2$) have been found for the vertex under examination ($\mathbf{v}_1$), the loop is defined as *open* since t_f Í t_l. In the case that there are other edges incident to $\mathbf{v}_1$ in the queue, the *front* and *back* columns of the *ptt* are emptied (figure 6g). Again, the first element of the queue is popped off ($\mathbf{e}_8$); the triangles $\mathbf{t}_1$ and $\mathbf{t}_6$ are added to the corresponding rows of the matrix of the vertices $\mathbf{v}_1$ and $\mathbf{v}_6$ (figure 6h). Once more, the first element of the new queue (figure 6i) is popped off ($\mathbf{e}_9$). Since one of the two triangles incident to the edge ($\mathbf{t}_4$) is a terminal point (*front*) of the loop, in the corresponding row of *ptt*, this triangle is substituted with the other ($\mathbf{t}_3$) (figure 6l). This procedure is iterated until the triangles of the *front* and the *back* column are the same for a vertex (figure 6m), or, in other words, the loop is *closed*. In the case that in the *deq* there are edges incident to that vertex (figure 6n), the corresponding triangles are erased (figure 6o). The procedure ends when the *deq* is empty.

5 EXPERIMENTAL RESULTS AND DISCUSSION

The methodology described in the previous sections has been implemented in original software, coded in C++. The method being proposed has been tested for the tessellation of several scanned point clouds characterised by different value and uniformity in sampling rate, geometries, topologies and noise level. Most of the test cases used are typical benchmarks taken from the related literature, although some others are artificially noised test cases purposely designed. All the tests have been run on a laptop with 1.86 GHz Intel Pentium M Processor and 1 GB RAM.

The performance of the algorithm has been assessed in terms of the tessellation rate ([ktriangles/s]) and the quality of the generated mesh. The latter has been analysed by evaluating:

- The mean value of the following quality factor of the generated triangles [35]:

$$QF = \frac{\sqrt{12}}{d}\sqrt{\frac{\prod_{i=1}^{3}(p-d_i)}{p}} \tag{5.1}$$

  where d_i is the length of the *i-th* side of the triangle, $d = \max_{i=1,2,3}(d_i)$ and $p = \sum_{i=1}^{3} d_i \Big/ 2$. The value of *QF* varies from 0 (for triangles having null area) to 1 (for equilateral triangles). This factor is very significant since uniform meshes characterised by equilateral triangles are required in most of the practical uses of tessellated surfaces.
- The mean value of the distance (μ_d%) of the unmeshed points from the tessellated surface, normalised on the mean spacing of the point cloud. Since the data points lie on the original surface and outliers are excluded, this index is an estimation of the error in meshing data points.
- The number of the following defects:
  - nonðmanifold vertices (n_{nmv});
  - nonðmanifold edges (n_{nme});
  - holes (n_{holes}): unmeshed areas;
  - boundary edges (n_{be}): edges bordering the holes.

The performance of the *Robust G2S* method is compared with that of the old one [27] (henceforth *G2S_old*) that of the *Cocone* methods (*Cocone* [15], *Tight Cocone* [16] and *Robust Cocone* [17]), whose implemented software has been kindly provided by the authors, and is also compared with our implementation of the *Ball Pivoting* [24]. The last two methods can be considered to be reference implementations of the Delaunay tessellation and of the mesh-growing approaches. In the following experiment the closed point clouds are analysed with the *Tight Cocone*, the open point clouds with the *Cocone* method and the noisy ones are tessellated by using the *Robust Cocone*. Neither the *G2S*s nor the *Cocone* family methods require any empirical input parameters. On the contrary, the *BPA* needs the ball pivoting radius. The *Ball Pivoting* performance is largely affected by the setting parameters which must be accurately defined to obtain satisfactory results but a tedious and time-consuming trialðand-error process is required.

5.1 Typical Benchmarks

The first set of experiments consists of the typical benchmarks used in the related literature to evaluate tessellation methods. In particular, 16 closed point clouds and 10 open point clouds, all of them having different geometries and having been scanned with different technologies, are considered. Eight of these point clouds have more than one million points and can be considered to be very large data sets. Figure 7 illustrates renderings of some test cases tessellated with the proposed method. The testing results are reported in table 1 ð 6.

Some of the benchmark test cases (*Neptune*, *Asian Dragon*, *Amphora* and *Thai Statue*) cannot be tested with the available *Cocone* and *Tight Cocone* implementations which cannot work for them.

When analysing the results obtained, it is easy to conclude that all the methods here considered fall short for point clouds (*Toywheel*, *Turtle* and *Galaad*) characterised by a strongly nonðuniform sampling.

The improvements introduced in *Robust G2S*, are achieved by a small reduction of the tessellation rate respect to the *G2S_old*. However, *Robust G2S* yields results which are, on average, about 300 times and 8 times higher than the *Cocone* and the *BPA* methods, respectively. Our implementation of the *BPA* shows a tessellation rate comparable with the implementation proposed in literature.

If we analyse the values for the *QF* index, the *Robust G2S* method is verified to produce triangles whose quality is similar (99.58%) to those obtained with the *Cocone* methods and slightly better than those obtained by means of the *Ball Pivoting* one (95.29%).

Generally speaking, the *Robust G2S* method (μ_d%=0.65%) and the *Cocone* methods (μ_d%=0.57%) can reproduce even the smallest details of well-sampled surfaces. On the contrary, and owing to difficulties in tessellating concave areas of point clouds, the *BPA* method produces many unmeshed points (μ_d%=21.45%). Figure 8 shows the maps of the μ_d% of the *Chinese_Dragon*. The *Robust G2S* reconstructs better the concave areas since, unlike the *BPA*, the ball radius is locally adapted to point spacing.

For all the cases analysed, the *Robust G2S* does not produce, as opposed to the other methods, non ð manifold vertices. Furthermore, when using the priority queue in the new version of G2S, in most cases there is a reduction of holes and boundary edges. In some cases, such as the *raptor,* the marked reduction in boundary edges is due to the elimination of the problem of twisting surface generation. Figure 9 shows the renderings of the tessellation obtained for the *Raptor* with both the *G2S_old* (a) and *Robust G2S*. In the same figure, the outside of triangles is coloured blue whereas the inside is coloured yellow. The *Robust G2S* performance is comparable with that of the *Cocone* family methods which are based on the Delaunay triangulation method, which is intrinsically more robust, but 300 times slower. The *Robust G2S* method generates defectiveness, essentially in those areas of the point clouds which cannot be considered to be locally flat since the sampling density is not accurate enough to reproduce surface details.

5.2 Noisy Point Clouds

In order to verify the performance of the *Robust G2S* in the tessellation of noised point cloud data, specific experiments are carried out. The performance of *Robust G2S* is compared with those of the *G2S_old* [27], *Robust Cocone* [17] and the *Ball Pivoting* [24].

The first experiment aims at comparing the four methods as regards the tessellation of the *Stanford Bunny* with different levels of noise added. Noise is randomly generated according to a Gaussian probability density distribution with different values of standard deviation expressed as percentage of the mean spacing of the original point cloud (ů%). Figure 10 illustrates the results of the renderings and table 7 reports the number of defects. In all the cases analysed, the *Robust G2S* method proves to be capable of reproducing even the smallest details of the model preventing non-manifold edges and vertices. On the contrary, the *Robust Cocone* and the *BPA* methods bring about a coarse reconstruction of the model and some important details are completely neglected. It is the case of the *Bunny Stanford* neck. For a high value of ů% (ů%>25%), the *Robust G2S* produces a tessellation with a high number of holes and boundary edges. Large random errors being applied to the original model destroy, depending on the ratio between error and point spacing, the characteristic regularity of the original surface to the extent it produces geometric nonsense. In these cases, the assumption of local flatness, which is basic to recognising the nature of a regular surface in a point cloud, is no longer valid.

The second set of experiments is carried out in order to compare the four methods as regards the tessellation of the point cloud with different number of outliers. For this purpose, in the *Stanford Bunny* outliers are randomly added according to the following percentages of the total number of points: 5%, 10% and 20%. The *Robust Cocone* seems to be inadequate to tessellate point clouds with this type of noise (figure 11). Due to the use of a relatively large ball, the *BPA* does not process as outliers any points which are external to the regular surface and produce the typical cones shown in figure 11. All in all, the *Robust G2S* shows good results thanks to the intrinsic characteristic of the method which tends to search for *candidate points* mainly in the regular growth of the surface. Furthermore, the *Robust G2S* does not generate non-manifold vertices (table 8) and the number of holes and boundary edges is similar to those produced by the *BPA* method.

6 CONCLUSION

In a previous paper [27] these authors had already presented a new-mesh growing approach based on the Gabriel 2 **ð** Simplex (G2S) criterion. The results obtained proved that the G2S is competitive in terms of tessellation rate, quality of the generated triangles and low defectiveness, especially when compared with the *Cocone* family and the *Ball Pivoting* methods. Its major limitation was that, in the presence of a mesh which was locally non **ð** flat or was not sufficiently sampled, it proved to be less robust and holes and non **ð** manifold vertices were generated. In order to improve the robustness of the *G2S* mesh-growing method, this paper proposes an original *priority queue* for the driving of the front growth and a post processing to efficiently erase the non **ð** manifold vertices. The performance of *Robust G2S* has been compared with that of *G2S_old*, and that of the *Cocone* family and the *Ball Pivoting* methods in the tessellation of some benchmark point clouds and artificially noised test cases. The results derived from these experiments show that the improvements proposed and implemented prevent the generation of non **ð** manifold vertices and make the *Robust G2S* more robust than *G2S_old* in terms of generation of defects such as holes and boundary edges, also in presence of noised point clouds. This performance improvement is achieved by a small reduction of the tessellation rate respect to the *G2S_old* method. However, the tessellation rate is still at least an order of magnitude higher than the *Cocone* family and the *Ball Pivoting* methods In the case of much noised meshes, *Robust G2S* produces more holes and boundary edges than the *Robust Cocone* and the *Ball Pivoting* methods, but the last named ones do not preserve important details of the object. Finally, in the presence of meshes with outliers, the number of holes and boundary edges produced by *Robust G2S* can be said to be comparable with those produced by the *Ball Pivoting* method.

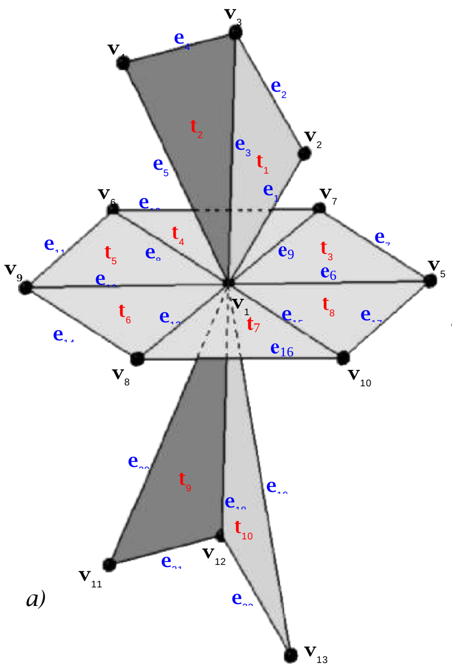

a)

deq				
e_l	p_f	p_l	t_f	t_l
$\mathbf{e}_3$	$\mathbf{v}_1$	$\mathbf{v}_3$	$\mathbf{t}_1$	$\mathbf{t}_2$
$\mathbf{e}_6$	$\mathbf{v}_1$	$\mathbf{v}_5$	$\mathbf{t}_3$	$\mathbf{t}_8$
$\mathbf{e}_8$	$\mathbf{v}_1$	$\mathbf{v}_6$	$\mathbf{t}_4$	$\mathbf{t}_5$
$\mathbf{e}_9$	$\mathbf{v}_1$	$\mathbf{v}_7$	$\mathbf{t}_3$	$\mathbf{t}_4$
$\mathbf{e}_{12}$	$\mathbf{v}_1$	$\mathbf{v}_9$	$\mathbf{t}_5$	$\mathbf{t}_6$
$\mathbf{e}_{13}$	$\mathbf{v}_1$	$\mathbf{v}_8$	$\mathbf{t}_6$	$\mathbf{t}_7$
$\mathbf{e}_{15}$	$\mathbf{v}_1$	$\mathbf{v}_{10}$	$\mathbf{t}_7$	$\mathbf{t}_8$
$\mathbf{e}_{18}$	$\mathbf{v}_1$	$\mathbf{v}_{12}$	$\mathbf{t}_9$	$\mathbf{t}_{10}$

b)

ptt			
v_l	*front*	*back*	$n_{t,a}$
$\mathbf{v}_1$			0
$\mathbf{v}_2$			0
$\mathbf{v}_3$			0
$\mathbf{v}_4$			0
$\mathbf{v}_5$			0
$\mathbf{v}_6$			0
$\mathbf{v}_7$			0
$\mathbf{v}_8$			0
$\mathbf{v}_9$			0
$\mathbf{v}_{10}$			0
$\mathbf{v}_{11}$			0
$\mathbf{v}_{12}$			0
$\mathbf{v}_{13}$			0

c)

ptt			
v_l	*front*	*back*	$n_{t,a}$
$\mathbf{v}_1$	$\mathbf{t}_1$	$\mathbf{t}_2$	2
$\mathbf{v}_2$			0
$\mathbf{v}_3$	$\mathbf{t}_2$	$\mathbf{t}_1$	2
$\mathbf{v}_4$			0
$\mathbf{v}_5$			0
$\mathbf{v}_6$			0
$\mathbf{v}_7$			0
$\mathbf{v}_8$			0
$\mathbf{v}_9$			0
$\mathbf{v}_{10}$			0
$\mathbf{v}_{11}$			0
$\mathbf{v}_{12}$			0
$\mathbf{v}_{13}$			0

d)

ptt			
v_l	*front*	*back*	$n_{t,a}$
$\mathbf{v}_1$			0
$\mathbf{v}_2$			0
$\mathbf{v}_3$			0
$\mathbf{v}_4$			0
$\mathbf{v}_5$			0
$\mathbf{v}_6$			0
$\mathbf{v}_7$			0
$\mathbf{v}_8$			0
$\mathbf{v}_9$			0
$\mathbf{v}_{10}$			0
$\mathbf{v}_{11}$			0
$\mathbf{v}_{12}$			0
$\mathbf{v}_{13}$			0

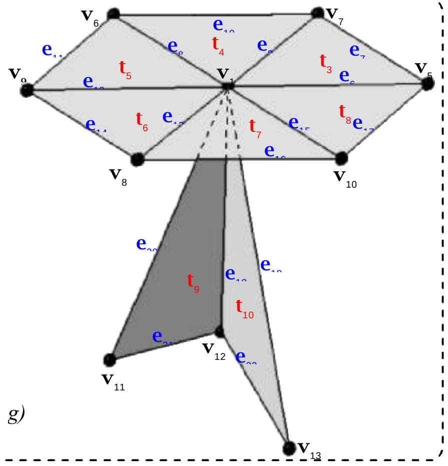

g)

deq				
e_l	p_f	p_l	t_f	t_l
$\mathbf{e}_6$	$\mathbf{v}_1$	$\mathbf{v}_5$	$\mathbf{t}_3$	$\mathbf{t}_8$
$\mathbf{e}_8$	$\mathbf{v}_1$	$\mathbf{v}_6$	$\mathbf{t}_4$	$\mathbf{t}_5$
$\mathbf{e}_9$	$\mathbf{v}_1$	$\mathbf{v}_7$	$\mathbf{t}_3$	$\mathbf{t}_4$
$\mathbf{e}_{12}$	$\mathbf{v}_1$	$\mathbf{v}_9$	$\mathbf{t}_5$	$\mathbf{t}_6$
$\mathbf{e}_{13}$	$\mathbf{v}_1$	$\mathbf{v}_8$	$\mathbf{t}_6$	$\mathbf{t}_7$
$\mathbf{e}_{15}$	$\mathbf{v}_1$	$\mathbf{v}_{10}$	$\mathbf{t}_7$	$\mathbf{t}_8$
$\mathbf{e}_{18}$	$\mathbf{v}_1$	$\mathbf{v}_{12}$	$\mathbf{t}_9$	$\mathbf{t}_{10}$

e)

deq				
e_l	p_f	p_l	t_f	t_l
$\mathbf{e}_8$	$\mathbf{v}_1$	$\mathbf{v}_6$	$\mathbf{t}_4$	$\mathbf{t}_5$
$\mathbf{e}_9$	$\mathbf{v}_1$	$\mathbf{v}_7$	$\mathbf{t}_3$	$\mathbf{t}_4$
$\mathbf{e}_{12}$	$\mathbf{v}_1$	$\mathbf{v}_9$	$\mathbf{t}_5$	$\mathbf{t}_6$
$\mathbf{e}_{13}$	$\mathbf{v}_1$	$\mathbf{v}_8$	$\mathbf{t}_6$	$\mathbf{t}_7$
$\mathbf{e}_{15}$	$\mathbf{v}_1$	$\mathbf{v}_{10}$	$\mathbf{t}_7$	$\mathbf{t}_8$
$\mathbf{e}_{18}$	$\mathbf{v}_1$	$\mathbf{v}_{12}$	$\mathbf{t}_9$	$\mathbf{t}_{10}$
$\mathbf{e}_6$	$\mathbf{v}_1$	$\mathbf{v}_5$	$\mathbf{t}_3$	$\mathbf{t}_8$

f)

ptt			
v_l	*front*	*back*	$n_{t,a}$
$\mathbf{v}_1$	$\mathbf{t}_4$	$\mathbf{t}_5$	2
$\mathbf{v}_2$			0
$\mathbf{v}_3$			0
$\mathbf{v}_4$			0
$\mathbf{v}_5$			0
$\mathbf{v}_6$	$\mathbf{t}_5$	$\mathbf{t}_4$	2
$\mathbf{v}_7$			0
$\mathbf{v}_8$			0
$\mathbf{v}_9$			0
$\mathbf{v}_{10}$			0
$\mathbf{v}_{11}$			0
$\mathbf{v}_{12}$			0
$\mathbf{v}_{13}$			0

h)

deq				
e_l	p_f	p_l	t_f	t_l
$\mathbf{e}_9$	$\mathbf{v}_1$	$\mathbf{v}_7$	$\mathbf{t}_3$	$\mathbf{t}_4$
$\mathbf{e}_{12}$	$\mathbf{v}_1$	$\mathbf{v}_9$	$\mathbf{t}_5$	$\mathbf{t}_6$
$\mathbf{e}_{13}$	$\mathbf{v}_1$	$\mathbf{v}_8$	$\mathbf{t}_6$	$\mathbf{t}_7$
$\mathbf{e}_{15}$	$\mathbf{v}_1$	$\mathbf{v}_{10}$	$\mathbf{t}_7$	$\mathbf{t}_8$
$\mathbf{e}_{18}$	$\mathbf{v}_1$	$\mathbf{v}_{12}$	$\mathbf{t}_9$	$\mathbf{t}_{10}$
$\mathbf{e}_6$	$\mathbf{v}_1$	$\mathbf{v}_5$	$\mathbf{t}_3$	$\mathbf{t}_8$

i)

ptt			
v_l	*front*	*back*	$n_{t,a}$
$\mathbf{v}_1$	$\mathbf{t}_3$	$\mathbf{t}_5$	3
$\mathbf{v}_2$			0
$\mathbf{v}_3$			0
$\mathbf{v}_4$			0
$\mathbf{v}_5$			0
$\mathbf{v}_6$	$\mathbf{t}_5$	$\mathbf{t}_4$	2
$\mathbf{v}_7$			0
$\mathbf{v}_8$			0
$\mathbf{v}_9$			0
$\mathbf{v}_{10}$			0
$\mathbf{v}_{11}$			0
$\mathbf{v}_{12}$			0
$\mathbf{v}_{13}$			0

l)

ptt			
v_l	*front*	*back*	$n_{t,a}$
$\mathbf{v}_1$	$\mathbf{t}_3$	$\mathbf{t}_3$	6
$\mathbf{v}_2$			0
$\mathbf{v}_3$			0
$\mathbf{v}_4$			0
$\mathbf{v}_5$	$\mathbf{t}_3$	$\mathbf{t}_8$	2
$\mathbf{v}_6$	$\mathbf{t}_5$	$\mathbf{t}_4$	2
$\mathbf{v}_7$	$\mathbf{t}_3$	$\mathbf{t}_4$	2
$\mathbf{v}_8$	$\mathbf{t}_6$	$\mathbf{t}_7$	2
$\mathbf{v}_9$	$\mathbf{t}_5$	$\mathbf{t}_6$	2
$\mathbf{v}_{10}$	$\mathbf{t}_7$	$\mathbf{t}_8$	2
$\mathbf{v}_{11}$			0
$\mathbf{v}_{12}$	$\mathbf{t}_9$	$\mathbf{t}_{10}$	2
$\mathbf{v}_{13}$			0

m)

deq				
e_l	p_f	p_l	t_f	t_l
$\mathbf{e}_{18}$	$\mathbf{v}_1$	$\mathbf{v}_{12}$	$\mathbf{t}_9$	$\mathbf{t}_{10}$

n)

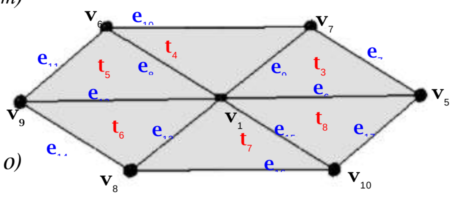

o)

Fig. 6: Explanation of the post processing used to erase the non ð manifold vertices.

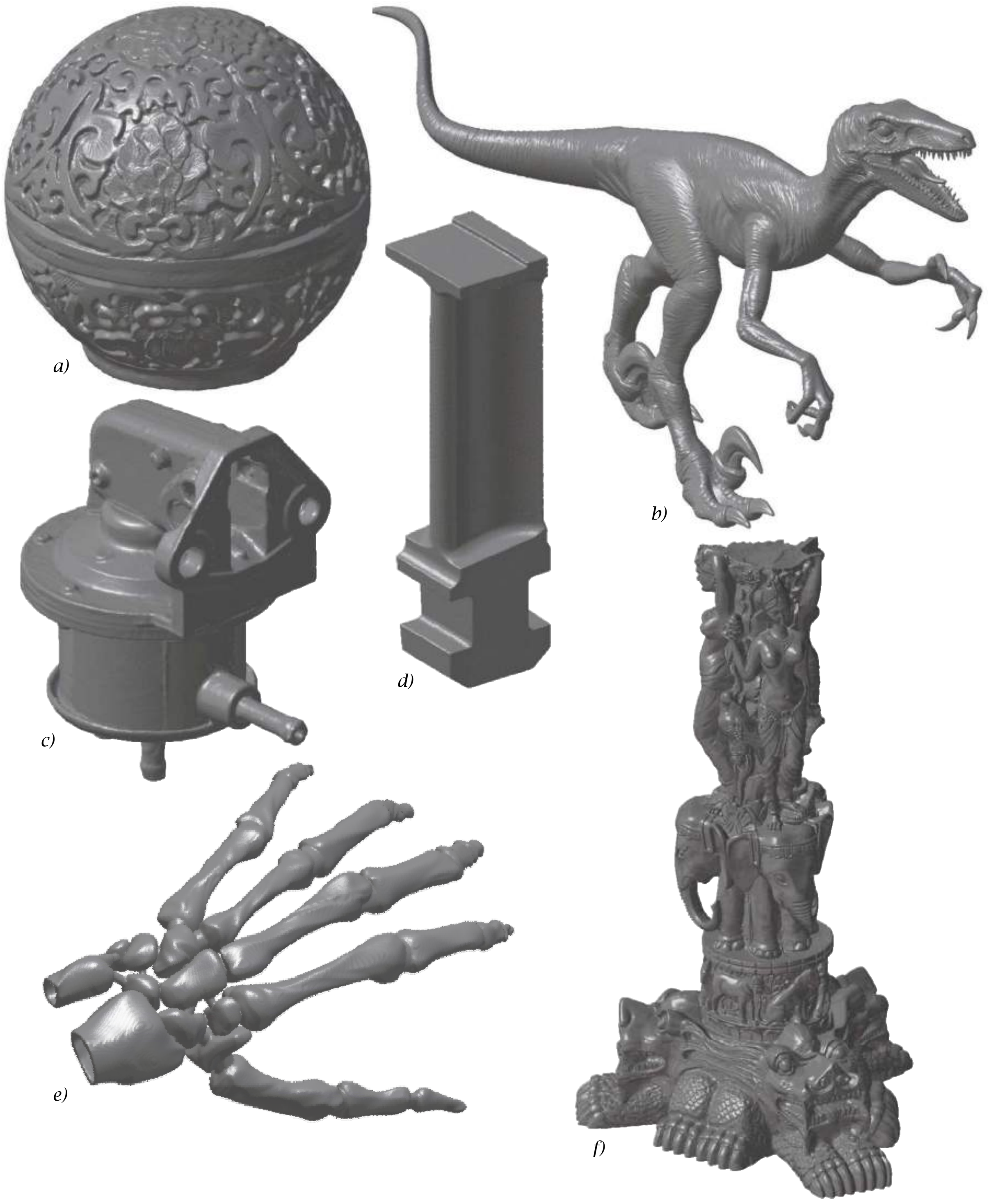

Fig. 7: Rendering of the following test cases: a) Red_circular_box; b) Raptor; c) Oil_pump; d) Turbine_blade2; e) Hand; f) Thai Statue.

Name	*No. of points*	*Robust G2S*		*G2S_old [27]*		*Tight Cocone [16]*		*Ball Pivoting [24]*	
		No. of triangles	*Rate [ktriangles/s]*	*No. of triangles*	*Rate [ktriangles/s]*	*No. of triangles*	*Rate [ktriangles/s]*	*No. of triangles*	*Rate [ktriangles/s]*
Rocker-arm (**)	10,044	20,084	320.9	20,084	380.1	20,088	1.33	18,848	26.18
Stanford Bunny (*)	35,947	71,873	294.3	71,884	321.7	71,884	0.99	67,449	22.86
Horse (**)	48,485	96,873	307.6	96,859	377.4	96,922	0.82	94,382	48.15
Armadillo (*)	172,975	345,897	303.0	345,934	372.8	345,944	0.85	307,286	33.18
Pulley (**)	293,672	587,266	328.5	587,181	371.8	587,312	0.67	571,738	52.82
Hand (**)	327,323	649,768	292.3	649,527	376.6	654,550	0.67	554,266	23.89
Turbine Blade 2 (****)	396,104	791,916	288.5	792,041	377.3	791,873	1.72	736,685	43.69
Dragon (***)	435,545	834,771	304.5	805,376	348.1	867,282	0.62	782,185	35.46
Bimba (**)	502,694	1,005,246	366.2	1,005,172	432.5	1,005,088	0.82	953,618	23.82
Happy Buddha (***)	543,652	1,038,953	338.0	1,004,540	351.0	1,081,232	0.51	809,539	25.36
Chinese Dragon (**)	655,980	1,311,307	322.0	1,311,296	475.2	1,310,435	0.99	966,266	25.28
Red_circular_box (**)	701,322	1,401,530	243.7	1,400,720	369.5	1,401,725	0.78	1,367,913	51.15
Turbine Blade (***)	882,954	1,740,362	351.9	1,759,357	364.4	1,759,514	1.11	1,630,254	47.28
Raptor (**)	1,000,080	1,685,915	349.6	1,716,226	439.6	1,854,921	0.28	1,378,599	43.48
Neptune (**)	2,003,933	4,007,522	261.8	4,007,628	362.8	- -	- -	3,119,149	20.01
Asian Dragon (*)	3,609,601	7,217,980	362.9	7,218,442	418.8	- -	- -	6,715,376	26.22

(*) http://www.graphics.stanford.edu/data/3Dscanrep/
(**) http://shapes.aimatshape.net/
(***) http://www.lodbook.com/models/
(****) http://www.scansystems.it

Tab. 1: Comparison between the performance of Robust G2S, G2S_old [27], Tight Cocone [16] and Ball Pivoting [24] in closed surfaces.

Name	*Robust G2S*		*G2S_old [27]*		*Tight Cocone [16]*		*Ball Pivoting [24]*	
	QF [26]	μ_d %	*QF [26]*	μ_d %	*QF [26]*	μ_d %	*QF [26]*	μ_d %
Rocker-arm	0.699	$1.40*10^{-2}$%	0.699	$1.40*10^{-2}$%	0.707	0,000%	0.651	5.46%
Stanford Bunny	0.708	0.007%	0.708	0.007%	0.713	0,029%	0.675	4.45%
Horse	0.714	0.51 %	0.714	0.51 %	0.714	0,42%	0.695	1.12%
Armadillo	0.768	0.000%	0.768	0.000%	0.775	0,005%	0.708	6.97%
Pulley	0.776	$5.39*10^{-3}$%	0.776	$5.39*10^{-3}$%	0.776	0,085%	0.761	3.77%
Hand	0.648	0.005%	0.648	0.005%	0.713	0,009%	0.620	180.0%
Turbine Blade 2	0.753	0.06%	0.753	0.06%	0.753	0,108%	0.698	1.68%
Dragon	0.642	1.63%	0.642	1.83%	0.622	0,819%	0.611	37.28%
Bimba	0.751	0.005%	0.751	0.194 %	0.751	0,322%	0.590	5.53%
Happy Buddha	0.613	0.145 %	0.613	0.145 %	0.614	1,39%	0.734	32.49%
Chinese Dragon	0.771	0.027%	0.771	0.027 %	0.769	0,208%	0.673	32.33%
Red_circular_box	0.785	0.038%	0.785	0.038%	0.783	0,053%	0.765	1.037%
Turbine Blade	0.585	0.68%	0.585	0.68 %	0.580	0,553%	0.580	70.01%
Raptor	0.723	11.52%	0.723	17.75%	0.704	7,345%	0,663	29.26%
Neptune	0.765	0.008%	0.765	0.008%	- -	- -	0.749	46.12%
Asian Dragon	0.903	0.012%	0.903	0.012%	- -	- -	0.887	7.81%

Tab. 2: Comparison between the quality reconstruction of Robust G2S, G2S_old [27], Tight Cocone [16] and Ball Pivoting [24] in closed surfaces.

Model name	*Robust G2S*				*G2S_old [27]*				*Tight Cocone [16]*				*Ball Pivoting [24]*			
			holes				*holes*				*holes*				*holes*	
	n_{nmv}	n_{nme}	n_{ho}	n_{be}	n_{nmv}	n_{nme}	n_{ho}	n_{be}	n_{nmv}	n_{nme}	n_{ho}	n_{be}	n_{nmv}	n_{nme}	n_{ho}	n_{be}
Rocker-arm	0	0	0	- -	0	0	0	- -	0	0	0	- -	2	0	5	54
Stanford Bunny	0	0	0	- -	0	0	0	- -	0	0	0	- -	1	0	0	0
Horse	0	0	7	83	0	0	8	149	0	0	1	4	11	0	6	111
Armadillo	0	0	0	- -	0	0	0	- -	0	0	0	- -	0	0	4	16
Pulley	0	0	1	4	0	1	2	10	0	0	0	- -	0	0	0	- -
Hand	0	0	13	90	0	0	19	126	8	0	6	58	0	0	32	186
Turbine Blade 2	0	0	2	9	0	10	12	77	1	0	1	11	0	0	1	3
Dragon	0	0	40	579	0	1	28	249	23	0	24	166	2	0	31	115
Bimba	0	0	6	117	0	11	12	220	8	0	5	54	0	0	0	- -
Happy Buddha	0	0	54	508	0	32	47	462	39	0	11	93	0	0	8	41
Chinese Dragon	0	0	19	103	0	47	35	928	18	0	13	119	0	0	12	40
Red_circular_box	0	0	97	635	0	27	42	327	12	0	10	75	53	0	501	6538
Turbine Blade	0	0	164	2089	0	42	66	1054	295	0	109	864	3	0	49	180
Raptor	0	0	36	207	0	269	91	1508	7751	0	4335	34781	0	0	7	37
Neptune	0	0	4	34	0	13	19	107	- -	- -	- -	- -	0	0	7	37
Asian Dragon	0	0	31	193	0	41	88	721	- -	- -	- -	- -	0	0	7	92

Tab. 3: Comparison between the defectiveness produced by Robust G2S, G2S_old [27], Tight Cocone [16] and Ball Pivoting [24] in closed surfaces.

Name	*No. of points*	*Robust G2S*		*G2S_old [27]*		*Tight Cocone [16]*		*Ball Pivoting [24]*	
		No. of triangles	*Rate [ktriangles/s]*	*No. of triangles*	*Rate [ktriangles/s]*	*No. of triangles*	*Rate [ktriangles/s]*	*No. of triangles*	*Rate [ktriangles/s]*
Foot (**)	10,010	19,970	310.8	19,972	352.9	19,982	2.25	18,332	37.05
Support (*)	549,007	1,096,742	322.5	1,097,412	397.6	1,097,538	1.82	1,074,677	49.65
Rolling Stage (**)	596,903	1,190,806	319.7	1,193,303	373.5	1,193,688	1.49	1,168,744	57.07
Body (****)	675,049	1,349,076	299.7	1,349,609	279.7	1,344,039	1.2	1,326,963	59.47
Nicolò da Uzzano (**)	946,760	1,891,949	367.0	1,891,992	464.5	1,891,669	1.93	1,795,917	40.33
Toy wheel (**)	1,001,231	- -	- -	- -	- -	1,702,234	0.41	959,810	0.27
Amphora (**)	1,317,152	2,590,549	274.6	2,616,596	295.9	- -	- -	2,544,331	62.67
Galaad (**)	1,451,502	- -	- -	- -	- -	2,215,146	0.53	272,561	0.47
Toy turtle (**)	1,472,131	- -	- -	- -	- -	2,226,103	0.60	670,035	0,53
Thai Statue (*)	4,999,997	9,994,088	275.1	9,994,088	303.8	- -	- -	8,335,937	19.48

(*) http://www.graphics.stanford.edu/data/3Dscanrep/
(**) http://shapes.aimatshape.net/
(***) http://www.lodbook.com/models/
(****) http://www.scansystems.it

Tab. 4: Comparison between the performance of Robust G2S, G2S_old [27], Tight Cocone [16] and Ball Pivoting [24] in open surfaces.

Name	*Robust G2S*		*G2S_old [27]*		*Tight Cocone [16]*		*Ball Pivoting [24]*	
	QF [26]	μ_d %	*QF [26]*	μ_d %	*QF [26]*	μ_d %	*QF [26]*	μ_d %
Foot	0.699	0.000%	0.699	0.000%	0.698	0.000%	0.682	4.66%
Support	0.730	0.237%	0.730	0.237%	0.729	0.013%	0.714	0.40%
Rolling Stage	0.616	0.006%	0.616	0.006%	0.616	0.005%	0.616	0.36%
Body	0.760	0.250%	0.760	0.250%	0.759	0.018%	0.739	0.58%
Nicolò da Uzzano	0.747	0.007%	0.747	0.007%	0.746	0.467%	0.707	5.1%
Toy wheel	--	--	--	--	0.492	4.69%	0.365	16.18%
Amphora	0.614	0.004%	0.614	0.004%	--	--	0.619	0.23%
Galaad	--	--	--	--	0.631	1.22%	0.444	817.77%

Toy turtle	--	--	--	--	0.635	17.72%	0.460	720.98%
Thai Statue	0.734	0.015%	0.734	0.015%	--	--	0.701	12.73%

Tab. 5: Comparison between the quality reconstruction of Robust G2S, G2S_old [27], Tight Cocone [16] and Ball Pivoting [24] in open surfaces.

Model name	*Robust G2S*				*G2S_old [27]*				*Tight Cocone [16]*				*Ball Pivoting [24]*			
			holes				*holes*				*holes*				*holes*	
	n_{nmv}	n_{nme}	n_{ho}	n_{he}	n_{nmv}	n_{nme}	n_{ho}	n_{he}	n_{nmv}	n_{nme}	n_{ho}	n_{he}	n_{nmv}	n_{nme}	n_{ho}	n_{he}
Foot	0	0	0	- -	0	0	0	- -	1	0	2	10	0	0	3	49
Support	0	0	7	43	0	85	21	57	14	0	2	8	0	0	13	159
Rolling Stage	0	0	1	5	0	3	6	28	3	0	5	36	0	0	0	- -
Body	0	0	8	49	0	166	25	336	87	0	30	161	0	0	50	354
Nicolò da Uzzano	0	0	1	4	0	1	0	- -	98	0	284	1289	41	0	12	94
Toy wheel	-	-	- -	- -	-	-	- -	- -	79073	2795	29542	206799	5755	0	4079	26105
Amphora	0	0	4	39	0	0	1	10	- -	- -	- -	- -	3	0	9	165
Galaad	-	-	- -	- -	-	- -	- -	-	141928	8945	47228	347125	126	0	164	873
Toy turtle	-	-	- -	- -	-	-	- -	- -	144735	10771	49255	354636	199	0	403	2418
Thai Statue	0	0	25	205	0	0	64	1348	- -	- -	- -	- -	1742	0	539	7068

Tab. 6: Comparison between the defectiveness produced by Robust G2S, G2S_old [27], Tight Cocone [16] and Ball Pivoting [24] in open surfaces.

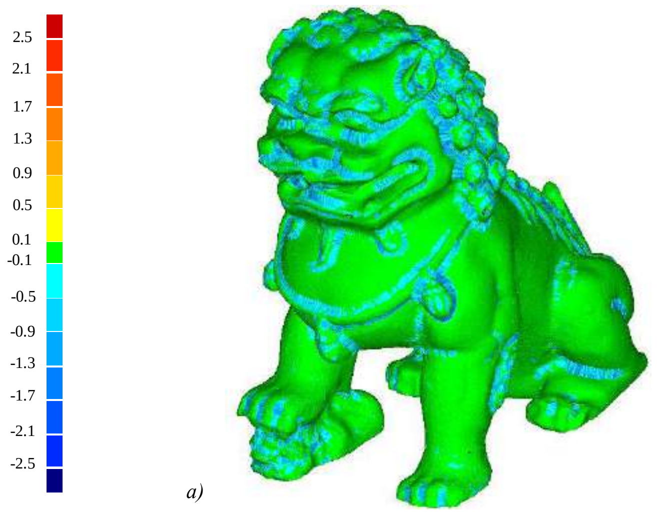

Fig. 8: Maps of the deviations between the original point cloud of the Chinese_Dragon mesh obtained by Ball Pivoting (a) and Robust G2S (b).

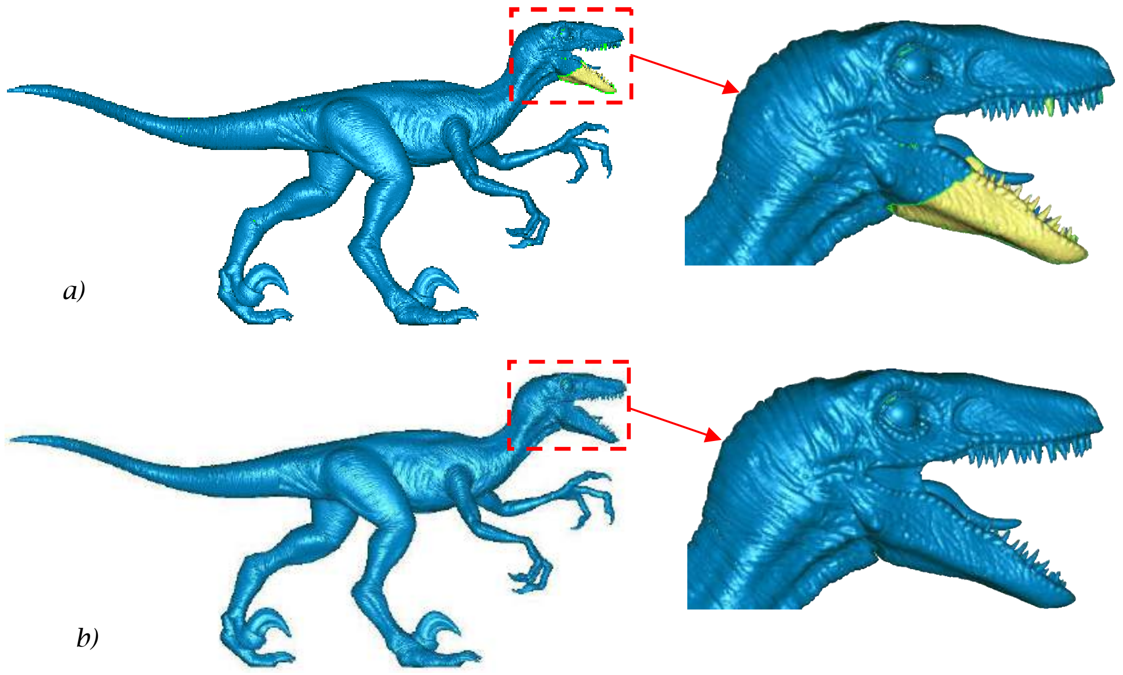

Fig. 9: Renderings of the tessellations obtained for the Raptor with the old (a) and the new versions of the G2S criterion.

	New G2S method	Old G2S method [27]	Robust Cocone method [17]	Ball Pivoting [24]
σ=10%	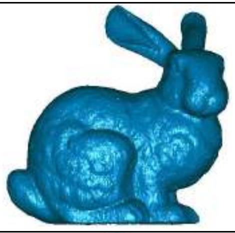	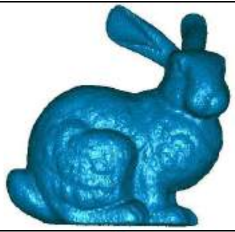	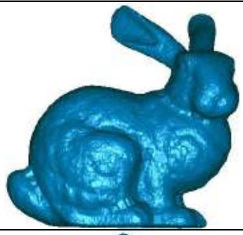	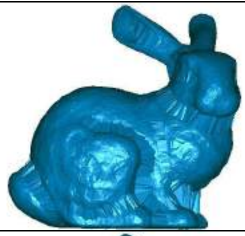
σ=25%	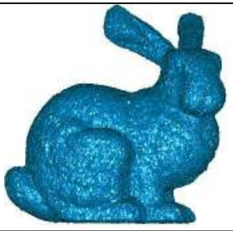	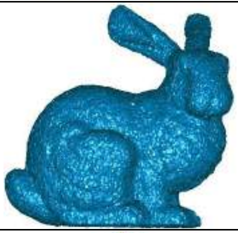	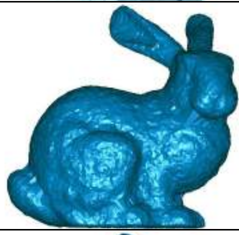	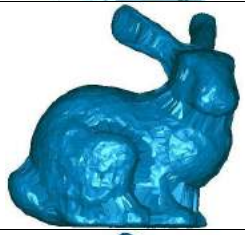
σ=50%	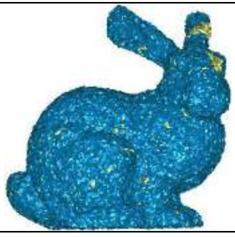	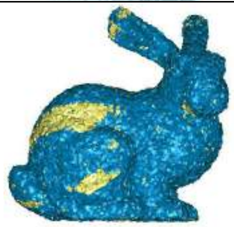	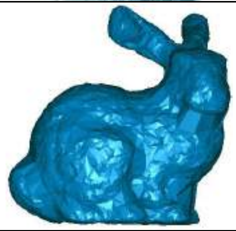	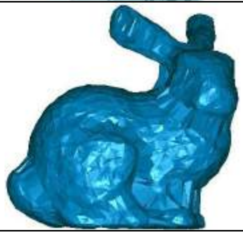

Fig. 10: Comparison between the two versions of the G2S, the Robust Cocone [17] and the Ball Pivoting [24] algorithms in the tessellation of noise added point clouds.

	New G2S method	Old G2S method [27]	Robust Cocone method [17]	Ball Pivoting [24]
5%	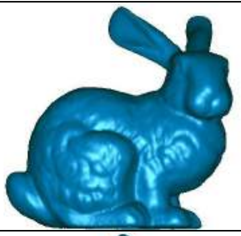	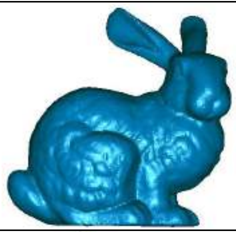	The exe program generates an empty file	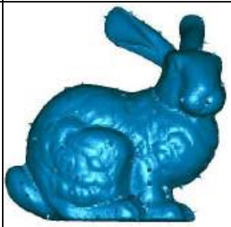
10%	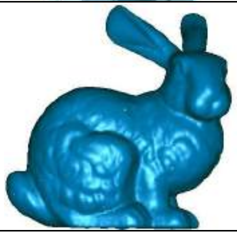	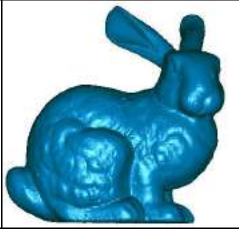	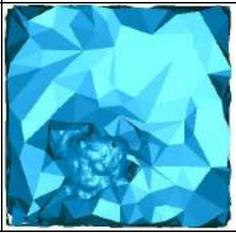	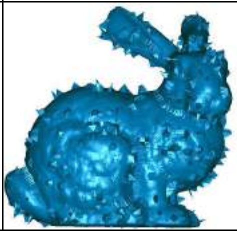

20%	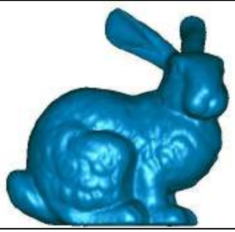	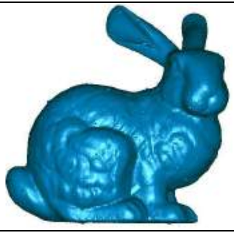	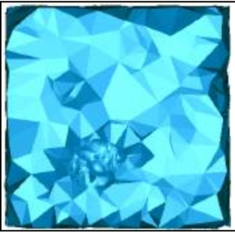	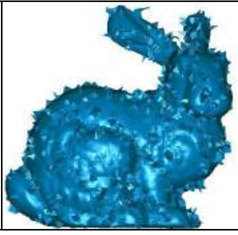

Fig. 11 Comparison between the two versions of the G2S, the Robust Cocone [17] and the Ball Pivoting [24] algorithms in the tessellation of point clouds with outliers added.

	New G2S Method			**Old G2S Method [27]**			**Robust Cocone method [17]**			**BPA method [24]**		
		holes			**holes**			**holes**			**holes**	
	n_{nm}	n_{holes}	n_{he}	n_{nm}	n_{holes}	n_{he}	n_{nm}	n_{holes}	n_{he}	n_{nm}	n_{holes}	n_{he}
σ=10%	0	0	- -	1	1	6	0	0	- -	0	0	- -
σ=25%	0	17	30	15	22	71	1	0	- -	0	3	9
σ=50%	0	241	1474	720	457	2967	1	0	- -	0	6	36

Tab. 7: Comparison of defectiveness generated by Robust Cocone [17] and Ball Pivoting [24] in the tessellation of noise added point clouds.

	Defectiveness generated											
	New G2S Method			**Old G2S Method [27]**			**Robust Cocone method [17]**			**BPA method [24]**		
		holes			**holes**			**holes**			**holes**	
	n_{nm}	n_{holes}	n_{he}	n_{nm}	n_{holes}	n_{he}	n_{nm}	n_{holes}	n_{he}	n_{nm}	n_{holes}	n_{he}
5%	0	0	- -	0	2	4	- -	- -	- -	7	11	149
10%	0	20	244	114	17	725	- -	- -	- -	13	34	206
20%	0	31	457	123	24	757	- -	- -	- -	12	45	326

Tab. 8: Comparison of defectiveness generated by Robust Cocone [17] and Ball Pivoting [24] in the tessellation of point clouds with outliers added.

REFERENCES

[1] Li, X.; Han, C.Y.; Wee, W. G.: On surface reconstruction: A priority driven approach. Computer-Aided Design, 41 (9), 2009, 626-640, http://dx.doi.org/10.1016/j.cad.2009.04.006.

[2] Chang, M. C.; Leymarie, F. F.; Kimia, B. B.: Surface reconstruction from point clouds by transforming the medial scaffold. Computer Vision and Image Understanding, 113 (11), 2009, 1130 ð 1146, http://dx.doi.org/10.1016/j.cviu.2009.04.001.

[3] Lorensen, W. E.; Cline, H. E.: Marching Cubes: A high resolution 3D surface construction algorithm. Computer Graphics, 21 (4), 1987, 163 ð 169, http://dx.doi.org/10.1145/37402.37422.

[4] Carr, J.; Beatson, R.; Cherrie, H.; Mitchel, T.; Fright, W.; Mccallum, B.; Evans, T.: Reconstruction and representation of 3D objects with radial basis functions. In Proceedings of the 28th annual conference on Computer graphics and interactive techniques (SIGGRAPH), 2001, 67ð76.

[5] Turk, G.; OöBrien, J.: Modelling with implicit surfaces that interpolate. ACM Transaction on Graphics, 21 (4), 2002, 855ð873, http://dx.doi.org/10.1145/571647.571650.

[6] Dey, T. K.; Sun, J.: An adaptive MLS surface for reconstruction with guarantees. In Proceedings of the third Eurographics symposium on Geometry processing, July 04-06, 2005, Vienna, Austria.

[7] Kolluri, R.: Provably good moving least squares. ACM Transactions on Algorithms, 4 (2), 2008, 1-25, http://dx.doi.org/10.1145/1361192.1361195.

[8] Yang, Z.; Seo, Y.H.; Kim, T.W.: Adaptive triangular-mesh reconstruction by mean-curvature-based refinement from point clouds using a moving parabolic approximation. Computer-Aided Design, 42 (1), 2010, 2-17, http://dx.doi.org/10.1016/j.cad.2009.04.014.

[9] Kazhdan, M.; Bolitho, M.; Hoppe, H.: Poisson surface reconstruction. In Symposium on Geometry Processing, 2006, 61ð70.

[10] Saleem, W.; Schall, O.; Patane, G.; Belyaev, A.;, Seidel, H.: On stochastic methods for surface reconstruction. International Journal of Computer Graphics, 23 (6), 2007, 381-395, http://dx.doi.org/10.1007/s00371-006-0094-3.

[11] Jalba, A.C.; Roerdink, J.B.T.: Efficient surface reconstruction using generalized coulomb potentials. IEEE Transactions on Visualization and Computer Graphics, 13 (6), 2007, 1512-1517, http://dx.doi.org/10.1109/TVCG.2007.70553.

[12] Yoon, M.; Lee, Y.; Lee, S.; Ivrissimtzis, I.; Seidel, H.-P.: Surface and normal ensembles for surface reconstruction. Computer-Aided Design 39 (5); 2007, 408-420, http://dx.doi.org/10.1016/j.cad.2007.02.008.

[13] Couprie, C.; Bresson, X.; Najman, L.; Talbot, H; Grady, L.: Surface reconstruction using Power Watershed. In Proceeding of International Symposium on Mathematical Morphology, 2011.

[14] Amenta, N.; Bern, M.; Kamvysselis, M.: A new Voronoi-Based Surface Reconstruction Algorithm. In the Proceeding of Computer Graphics (SIGGRAPH ô98), 1998, 415 ð 421.

[15] Amenta, N.; Choi, S.; Dey, T. K.; Leekha, N.: A simple algorithm for homeomorphic surface reconstruction. International Journal of Computational Geometry & Applications, 12 (1 & 2), 2007, 125 ð 141.

[16] Dey, T.K.; Goswami, S.: Tight cocone: A watertight surface reconstructor. Journal of Computing and Information Science in Engineering, 3 (4), 2003, 302ð307, http://dx.doi.org/10.1115/1.1633278.

[17] Dey, T.K.; Goswami, S.: Provable surface reconstruction from noisy samples. Computational Geometry, 35 (1 ð 2), 2006, 124 ð141, http://dx.doi.org/10.1016/j.comgeo.2005.10.006.

[18] Dey, T.K.; Giesen, J.; Hudson, J.: Delaunay based shape reconstruction from large data. In the Proceeding of the IEEE Symposium on Parallel and Large-Data Visualization and Graphics, 2001, 19ð27, http://dx.doi.org/10.1109/PVGS.2001.964399.

[19] Amenta, N.; Choi, S.; Kolluri, R.: The Power Crust, In the proceeding of the ACM Symposium on Solid Modeling and Applications, 2001, 249-260.

[20] Cohen-Steiner, D.; Da, F.: A greedy Delaunay-based surface reconstruction algorithm. The Visual computer, 20 (1), 2004, 4-16, http://dx.doi.org/10.1007/s00371-003-0217-z.

[21] Ma, J.; Feng, H.Y.; Wang, L.: Delaunay-based triangular surface reconstruction from points via Umbrella Facet Matching. In Proceeding of 6th Annual IEEE Conference On Automation Science and Engineering, 2010, 580-585.

[22] Gopi, M; Krishnan, S.; Silva, C.: Surface reconstruction using lower dimensional localized Delaunay triangulation. In the Proceeding of Eurographics, 19 (3), 2000, 467 - 478.

[23] Cazals, F.; Giesen, J.: Delaunay triangulation based surface reconstruction. In Effective Computational Geometry for Curves and Surfaces, Boissonnat J., Teillaud M., (Eds.). Springer-Verlag, Math. and Visualization, 2006, 231ð276, http://dx.doi.org/10.1007/978-3-540-33259-6_6.

[24] Bernardini, F.; Mittleman, J.; Rushmeier, H.; Silva, C.; Taubin, G.: The ball-pivoting algorithm for surface reconstruction. IEEE Transactions on Visualization and Computer Graphics, 5 (4), 1999, 349-59, http://dx.doi.org/10.1109/2945.817351.

[25] Huang, J.; Menq, C. H.: Combinatorial manifold mesh reconstruction and optimization from unorganized points with arbitrary topology. Computer ð Aided Design, 34 (2), 2002, 149ð65, http://dx.doi.org/10.1016/S0010-4485(01)00079-3.

[26] Lin, H. W.; Tai, C. L.; Wang, G.-J.: A mesh reconstruction algorithm driven by an intrinsic property of point cloud. Computer-Aided Design, 36 (1), 2004, 1ð9, http://dx.doi.org/10.1016/S0010-4485(03)00064-2.

[27] Di Angelo, L.; Di Stefano, P.; Giaccari, L.: A new mesh-growing algorithm for fast surface reconstruction. Computer ð Aided Design, 43 (6), 2011, 639-650, http://dx.doi.org/10.1016/j.cad.2011.02.012.

[28] Adamy, U.; Giesen, J.; John, M.: New techniques for topologically correct surface reconstruction. In the Proceedings of the conference on Visualization õ00, 2000, Los Alamitos, CA, USA, 373ð380, IEEE Computer Society Press, http://dx.doi.org/10.1109/VISUAL.2000.885718.

[29] Dyer, R.; Zhang, H.; Möller, T.: Observations on Gabriel meshes and Delaunay edge flips. Tech. Rep. TR 2008-22, 2008, Simon Fraser University. SFU-CMPT.

[30] Ruiz, O. E.; Cadavid, C.; Lalinde, J. G.; Serrano, R.; Peris-Fajarnes, G.: Gabriel-constrained parametric surface triangulation. Proceedings of World Academy of Science, Engineering, and Technology, 34, 2008, 578ð585.

[31] Hoppe, H.; Derose, T.; Duchamp, T.; McDonald, J.; Stuetzle, W.: Surface reconstruction from unorganized point clouds. In ACM SIGGRAPH, 1992, 71-78, http://dx.doi.org/10.1145/142920.134011.

[32] Turk, G.; Levoy, M.: Zippered polygon meshes from range images. In ACM SIGGRAPH, 1994, 311-318.

[33] Guéziec A.; Taubin G.; Lazarus F.; Horn B.: Cutting and stitching: Converting sets of polygons to manifold surfaces. IEEE Transactions on Visualization and Computer Graphics, 7(2), 2001, 136ð151, http://dx.doi.org/10.1109/2945.928166.

[34] Campen M.; Attene M.; Kobbelt L.: A Practical Guide to Polygon Mesh Repairing, Eurographics 2012 Tutorial.

[35] Bèclet, E.; Cuilliere, J. C.; Trochu, F.: Generation of a finite element MESH from stereolithography (STL) files. Computer-Aided Design, 34 (1), 2002, 1-17, http://dx.doi.org/10.1016/S0010-4485(00)00146-9.